

Microstructural evolution in copper subjected to severe plastic deformation: Experiments and analysis

A. Mishra ^a, B.K. Kad ^b, F. Gregori ^c, M.A. Meyers ^{a,*}

^a Department of Mechanical and Aerospace Engineering, Materials Science and Engineering Program, University of California, San Diego, 9500 Gilman Drive, La Jolla, CA 92093-0411, USA

^b Department of Structural Engineering, University of California, San Diego, La Jolla, CA, USA

^c Laboratoire des Propriétés Mécaniques et Thermodynamiques des Matériaux (CNRS), Université de Paris 13, France

Received 24 January 2006; received in revised form 14 July 2006; accepted 22 July 2006
Available online 27 October 2006

Abstract

The evolution of microstructure and the mechanical response of copper subjected to severe plastic deformation using equal channel angular pressing (ECAP) was investigated. Samples were subjected to ECAP under three different processing routes: B_C, A and C. The microstructural refinement was dependent on processing with route B_C being the most effective. The mechanical response is modeled by an equation containing two dislocation evolution terms: one for the cells/subgrain interiors and one for the cells/subgrain walls. The deformation structure evolves from elongated dislocation cells to subgrains to equiaxed grains with diameters of ~200–500 nm. The misorientation between adjacent regions, measured by electron backscatter diffraction, gradually increases. The mechanical response is well represented by a Voce equation with a saturation stress of 450 MPa. Interestingly, the microstructures produced through adiabatic shear localization during high strain rate deformation and ECAP are very similar, leading to the same grain size. It is shown that both processes have very close Zener–Hollomon parameters ($\ln Z \sim 25$). Calculations show that grain boundaries with size of 200 nm can rotate by ~30° during ECAP, thereby generating and retaining a steady-state equiaxed structure. This is confirmed by a grain-boundary mobility calculation which shows that their velocity is 40 nm/s for a 200 nm grain size at 350 K, which is typical of an ECAP process. This can lead to the grain-boundary movement necessary to retain an equiaxed structure.

© 2006 Acta Materialia Inc. Published by Elsevier Ltd. All rights reserved.

Keywords: Ultrafine grain metals; ECAP; Severe plastic deformation

1. Introduction

In recent years, severe plastic deformation has been a topic of widespread research owing to its capability of producing ultrafine-grained materials. Indeed, three entire conferences, the NanoSPD series [1–3], were devoted entirely to this theme. This topic is reviewed by Furukawa et al. [4]. Equal channel angular pressing (ECAP) is one of the variants of severe plastic deformation that is showing most promise because of its simplicity [5–8]. Grains of ~200 nm with a fairly equiaxed distribution can be obtained using an optimized processing route.

ECAP involves the use of a die that contains two intersecting channels of equal cross-section. The strain that the sample experiences is dependent on two parameters: the inner angle of intersection of the channels, Φ , and outer angle of curvature, Ψ [9]. Among the incentives for using this technique, the most important one is that the sample cross-section remains unchanged during processing. The microstructure after a certain number of passes is strongly dependent on the rotation scheme [10–12]. The most widely used rotation schemes are: route A, where the billet is not rotated between consecutive passes; route B_A, where the billet is rotated by 90° in alternate directions between consecutive passes; route B_C, where the billet is rotated by 90° in the same direction between consecutive passes; and route C, where the billet is rotated by 180° between consecutive

* Corresponding author. Tel.: +1 858 534 4719.

E-mail address: mameyers@mae.ucsd.edu (M.A. Meyers).

passes [13]. Studies on samples produced by these rotation schemes have shown that route B_C is the most effective route for producing an equiaxed microstructure [14,12,15,10]. However, it should be mentioned that conflicting results have been reported (e.g. [16]).

There has been considerable recent effort devoted to defect structures and constitutive modeling of the response of copper to severe plastic deformation. These efforts have involved careful dislocation density measurements by Ungar, Zehetbauer and co-workers [17–19]. Based on this work, Goerdeler and Gottstein [20] and Baik et al. [21,22] developed constitutive equations including hardening contributions from both cell interior and walls. Goerdeler and Gottstein [20] considered both dislocation generation and annihilation. Toth et al. [23] developed a dislocation-based model for all hardening stages in large strain deformation that involved the evolution of the volume fraction of cell walls which decreases with the deformation and gives rise to a plateau-like behavior.

In spite of the large number of papers, over 100, dedicated to ECAP, little effort has been directed toward elucidating the mechanism of ultrafine grain formation. A notable exception is the recent work by Xu et al. [24]. The research results presented herein had as a major goal the identification of the mechanisms of grain-size refinement.

2. Experimental methods

ECAP dies with two different values of ϕ (the inner angle of channel intersection), 90° and 102° , were used for our experiments. As opposed to the widely used single piece or vertical split die, we used a design where the split was horizontal. This enabled replacement of the lower block with channels of different angles while the top piece was still reusable. In both dies, the outer arc of curvature, Ψ , was 20° .

The shear strain per pass was equal to 0.87 for $\phi = 102^\circ$ and 1 for $\phi = 90^\circ$. With the exception of the entry and exit points, the channel diameter was uniformly 0.95 cm. The diameter was slightly enlarged at the entry and exit points to permit easy reinsertion of the sample in the channel. The initial samples of commercially pure Cu (purity <99.9%) were cut into billets of 6.5 cm length and 0.925 cm diameter that permitted a loose fit in the channel. Pressing was carried out using a H-13 tool steel plunger guided by a hydraulic press. The tolerance of the plunger was kept extremely low to prevent material from flowing between the walls of the channel and the plunger. Since the length of the channel was 15 cm, two samples were inserted in the channel at the same time. Each Cu sample was alternated with an Al sample to reduce friction along the channel walls. It was found that successive Cu samples required a much higher load than intercalated Cu and Al samples. The Al samples went through the channel smoothly with a very low applied load, while the load was needed to push the Cu sample through was significantly higher. For the

102° die, a compressive stress of ~ 1.52 GPa was required for the first two passes, while subsequent passes needed ~ 1.27 GPa. For the 90° die, the first two passes required ~ 2.54 GPa, while for subsequent passes the stress on the plunger dropped to ~ 1.9 GPa. This is close to the strength of the H-13 tool steel. The billets and plunger were well lubricated before pressing. All modifications were primarily aimed at reducing friction since that is the main deterrent and led to several die and plunger failures in our initial efforts.

Transmission electron microscope (TEM) analysis was carried out on a 200 kV JEOL (JEM-2010, LaB₆). Observations were made on both transverse (y) and longitudinal (x or z – no distinction was made between the two) directions. Crystallographic orientation analysis (using electron backscatter diffraction (EBSD)) was done with a TSL setup on a Stereoscan 360 (Cambridge Instruments). The scanning parameters were set such that a grain boundary was defined when the misorientation between adjacent measurement points was greater than 5° . As a result, grain size, as predicted from EBSD data, is shown to be larger than the actual value. To ensure precision, these results were used in combination with TEM to determine the correct value. For samples subjected to two or more passes, the measurement step size was reduced from 0.5 to 0.2 μm to capture the microstructural features. This led to a reduction of the scanning area to $50 \times 50 \mu\text{m}$ to complete the experiment in a reasonable time.

3. Results and discussion

3.1. Mechanical testing

Fig. 1 gives the Vickers hardness as a function of number of passes. The plot presents data from different sources [21,25–30,71]. The samples were processed with a 90° die

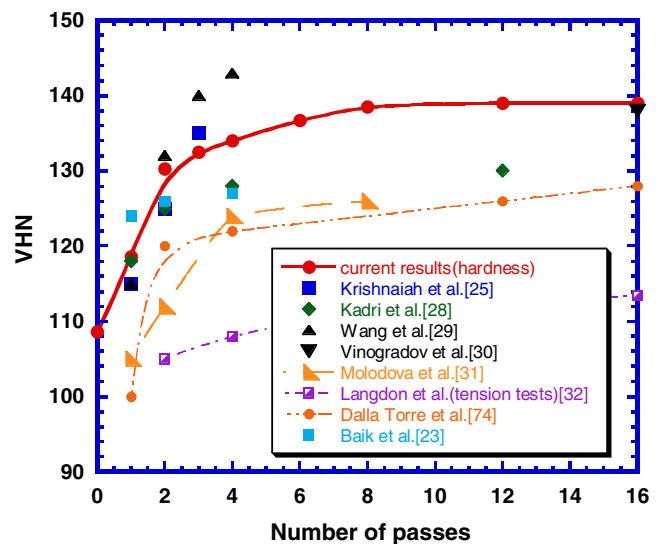


Fig. 1. Plot of hardness as a function of number of ECAP passes (data from different sources [21,25–30,72]).

using route B_C. As can be clearly seen, hardness saturates at eight passes. There is reasonable agreement between different researchers. The results by Langdon et al. [24] are somewhat lower because we converted their yield stress (in tension) to hardness by multiplying it by 3. The saturation is connected to the lower limit of the grain size achieved by ECAP which seems to be in the range of ~200 nm. If one applies the Hall–Petch equation one can infer a grain size from the value of the yield stress. There is some variation in the literature regarding the Hall–Petch slope, and one obtains $d = 690$ nm from Feltham and Meakin [31], $d = 428$ nm from Gourdin and Lassila [32], $d = 375$ nm from Andrade et al. [34], and $d = 67$ nm from Armstrong [35]. The above values are presented in Table 1.

Two initial conditions were used: an annealed and a work-hardened one. The results of compression tests are presented in Fig. 2. The two-pass sample showed a significant jump in strength over the initial sample. The rise in strength on higher number of passes was not as significant as it was for the first two passes. This is suggestive of the fact that the bulk of grain refinement happens in the first few passes. As will be discussed later, this was supported by EBSD data on grain size measurement distribution which yielded a steep decline in the grain size down to ~200 nm on the first few passes while additional passes simply increased the fraction of grains in this size range. It was also observed that the effect of initial state of specimen (annealed vs. cold worked) did not affect the mechanical response significantly. After two passes, the effects of initial microstructure are essentially eliminated.

Tensile tests were conducted on ECAP samples that were annealed at 700 °C for 1 h before processing. The initial sample showed a large ductility. Work hardening in the process of severe plastic deformation caused a large decrease in ductility of the ECAP samples, as can be seen in Fig. 3. The samples necked at strains of 2–3%. There was, as expected, a significant increase in strength of the ECAP samples over the initial sample.

Langdon et al. [30] introduced the Voce equation to describe the hardening in ECAP of aluminum and found that it reproduces the experimental results well for two or more passes, while the Ludwik–Hollomon equation represented the early response results. Accordingly, the Voce [36] equation was used in this work. It should be mentioned that this is merely an engineering fit equation without physical significance. Physically based constitutive equations are presented in Section 3.3. The mechanical response was modeled by

Table 1
Calculated grain sizes from the Hall–Petch relationship

References	k (GPa $\times 10^{-4}$ m ^{1/2})	d (grain size)
Feltham and Meakin [31]	3.53	690 nm
Gourdin and Lassila [32]	2.78	428 nm
Wang and Murr [33]	5.80	1.8 μ m
Andrade et al. [34]	0.56–2.6	375 nm
Armstrong [35]	1.1	67 nm

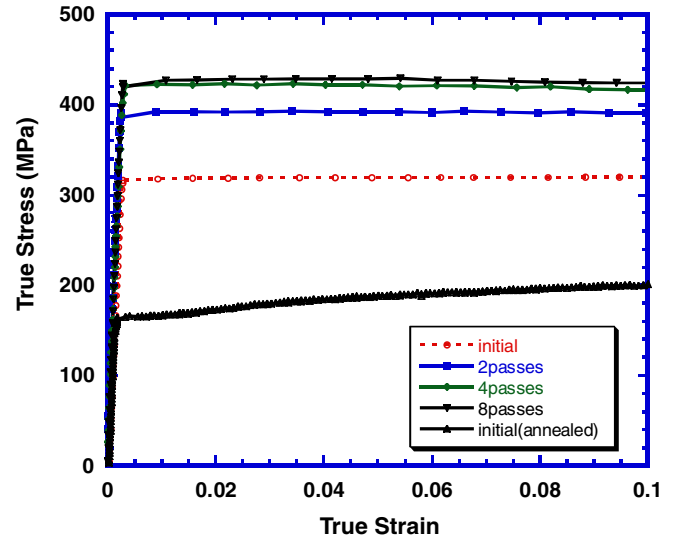


Fig. 2. Compression test results for samples ranging from initial to 8 passes at a strain rate of 0.1/s.

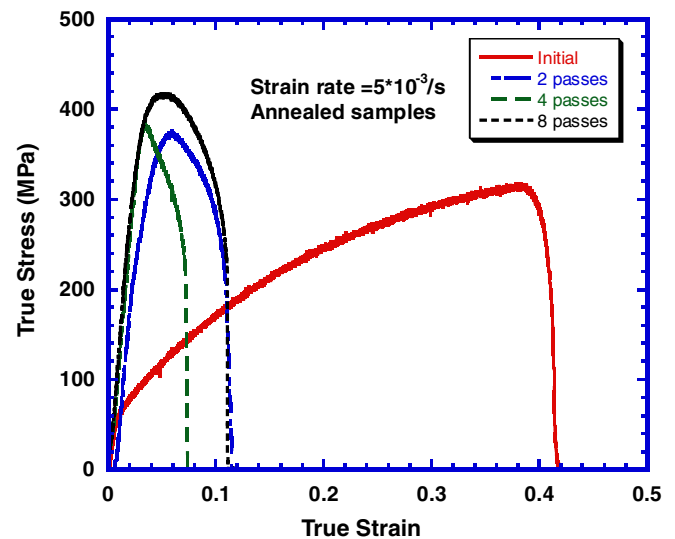


Fig. 3. Tensile test results of initial and ECAP samples. The samples were annealed at 700 °C for 1 h before processing.

$$\frac{\sigma_s - \sigma}{\sigma_s - \sigma_0} = \exp\left(-\frac{\varepsilon}{\varepsilon_c}\right), \quad (1)$$

where σ_0 is the initial yield stress, σ_s is the saturation stress and ε_c is a characteristic strain.

The yield strength of the ECAP samples was calculated from the hardness, using the expression $\sigma_y = H/3$, assuming that there is no work hardening. True strains in the ECAP samples were obtained from the shear strain (~1 in every ECAP pass) using the following relationship:

$$\varepsilon_t = \ln\left(\frac{(2 + 2\gamma + \gamma^2)^{1/2}}{\sqrt{2}}\right). \quad (2)$$

From the plotted values of yield strength as a function of true strain, the value of ε_c in the Voce equation was computed. Fig. 4a shows results from experiments and predic-

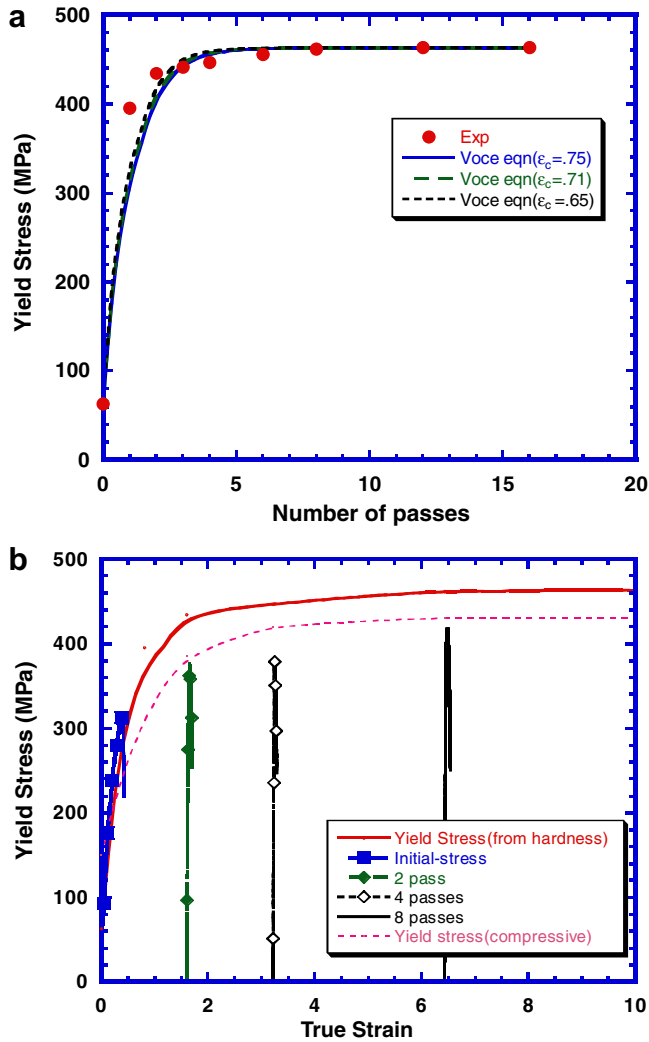


Fig. 4. (a) Voce equation and experimental results on yield stress as a function of number of ECAP passes. (b) Hardness, compressive and tensile test results combined.

tions from the Voce equation. The Voce equation captures the response from experimental results fairly well after two passes with the following values: $\sigma_s = 450$ MPa; $\varepsilon_c = 0.65$ – 0.75 . Fig. 4b shows the combined results expressed as true stress–true strain response from hardness, compressive and tensile testing. On the abscissa, the strain accumulated during ECAP was taken in account for the tensile testing samples. The lower values of the tensile strengths are in agreement with the results of Langdon et al. [24].

3.2. Fracture

Fig. 5a and b shows the fracture surface of the initial and eight-pass ECAP material, respectively (tensile specimens). The fractographs show, at the bottom of the dimples, holes which are the initiation sites for fracture. There is no significant difference in the dimple size between the two fractographs, in spite of the two orders of magnitude difference in grain size. The interpretation for the sim-

ilarity in the fracture morphology is that the initiation sites (in this case, most probably inclusions) have a similar distribution for the two conditions, since the material composition is the same. Therefore, knowing that the fracture morphology is dictated by the inclusions, it is reasonable to assume that the dimple size will be the same. This is shown in schematic fashion in Fig. 5c and d which shows a distribution of inclusions leading to dimples, independent of grain size. Nevertheless, the dimples seem to be shallower for the ultrafine-grained material. This is a direct consequence of the decreased ductility.

3.3. Microstructural evolution

ECAP specimens were examined by TEM in the longitudinal and transverse directions. The microstructures after 0, 2, 4 and 8 passes (90° die) using route B_C are shown in Fig. 6. As can be seen from the transverse microstructures, the grains are fairly equiaxed and a significant amount of grain breakdown process has taken place in the first two passes. The initial grain size is $30 \mu\text{m}$ while after two passes a significant fraction of the grains is below 200 nm . On additional passes, the amount of grains in the ultrafine range increases. The longitudinal section microstructures showed elongated grains after the first few passes, but for higher numbers of passes, these elongated grains break down to finer equiaxed grains. We postulate a mechanism of grain refinement in Section 3.6.

The evolution of microstructure in ECAP is dependent on the deformation path. Different processing routes lead to different final microstructures. In this work, three schemes were used: A (no rotation), C (180° rotation between passes) and B_C (90° rotation between passes). Fig. 7 shows micrographs of the transverse sections of three ECAP sequences processed to eight passes using these three routes. As can be clearly seen, routes A and C result in elongated grains while the distribution is fairly equiaxed in the sample processed via route B_C . The texture resulting from each of these processing routes after eight passes is shown in Fig. 8. The left-hand side shows the orientation images of the three transverse sections. It is clear that route B_C shows a more broken-up microstructure. It should be emphasized that grain boundaries with misorientations below 5° are not seen. The misorientation angle distributions (number fraction of grains) for each of these processing routes are also shown in Fig. 8. The texture evolved to (101) in both routes B_C and route A while it was dominantly (111) for route C.

The misorientation angle distribution (number fraction of grains) as a number of ECAP passes is shown in Fig. 9. For two passes, the fraction of boundaries that is low angle increases significantly, while large angle boundaries become a small fraction. This is a clear indication of the formation of cells and subgrains in the existing grains. For four passes, the misorientation between the subgrain increases, and there is a balanced distribution of low-angle and high-angle boundaries. After eight passes,

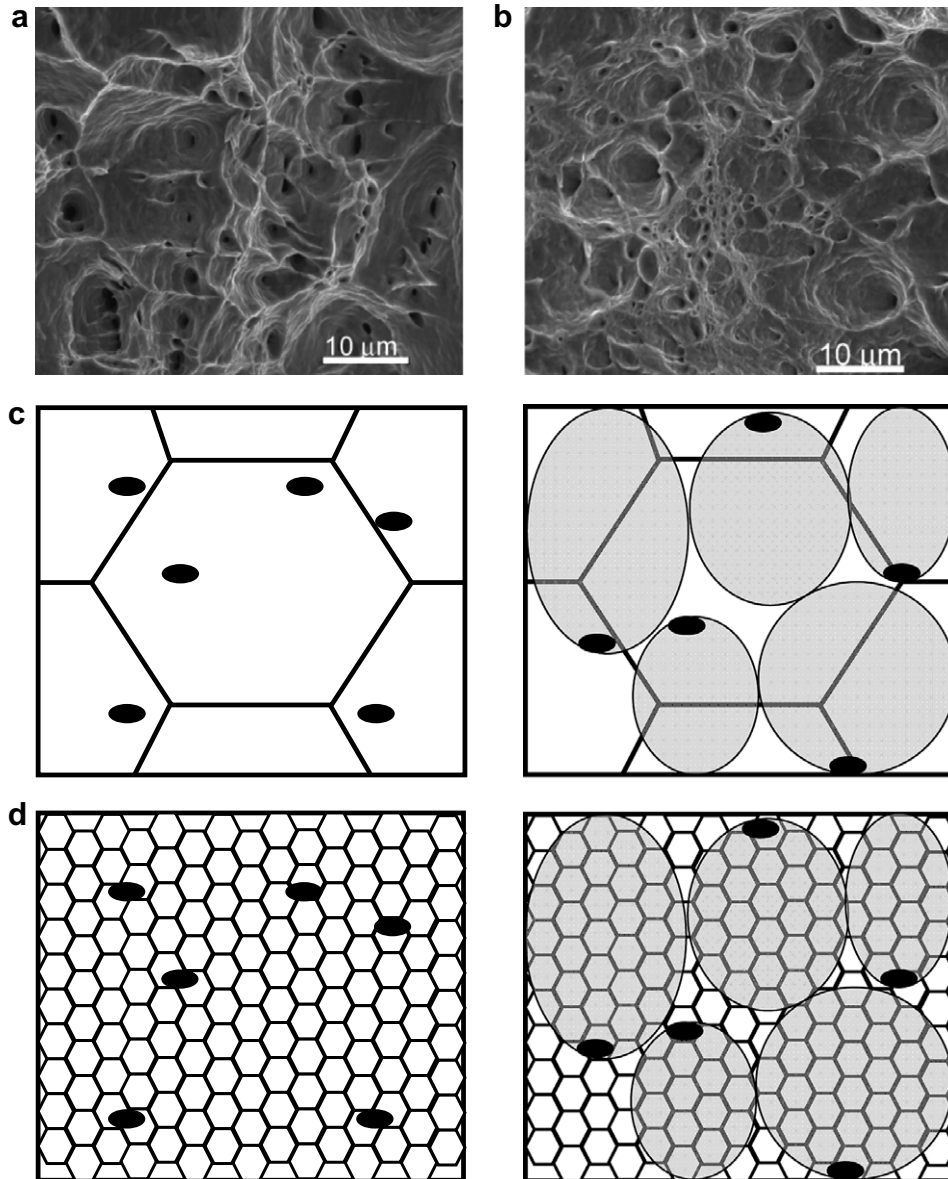


Fig. 5. SEM micrographs of (a) initial annealed polycrystalline sample and (b) ultrafine-grained Cu after 8 ECAP passes; (c, d) schematic explaining similarity in fracture features of coarse-grained and ultrafine-grained copper.

the low-angle grain boundaries are a minority, and the orientation distribution is similar to the initial one.

The Voce equation used in Section 3.1 is purely phenomenological and does not have a physical basis. The constitutive description of the microstructural evolution during ECAP is quite complex. Indeed, the microstructure after four passes is characteristic of Stage IV work hardening, with the cell walls becoming gradually thinner and the misorientation between neighboring subgrains gradually increasing. The dislocation density has been shown to saturate at an effective strain of 4, to a value of $15.2 \times 10^4/\text{m}^2$ by Ungar and Zehetbauer [17]. The flow stress has been expressed as a function of the dislocation density in an equation incorporating dislocation generation, storage and annihilation by Goerdeler and Gottstein [20]. In

ECAP, Baik et al. [21] developed a similar expression (Eq. (3)), separating the dislocation density in cell interior (ρ_c) and boundary (ρ_w), and incorporating the strain rate sensitivity in a manner similar to Goerdeler and Gottstein [20]:

$$\tau = \alpha G b \left(\frac{\dot{\gamma}}{\dot{\gamma}_0} \right)^{1/m} [f \sqrt{\rho_w} + (1-f) \sqrt{\rho_c}], \quad (3)$$

where f is the fraction of cell boundaries, and $\dot{\gamma}$ and $\dot{\gamma}_0$ are the actual and reference strain rates, respectively. The experimental cell size measurements from the current research and those of Baik et al. [21] (Fig. 10a) are in good agreement. Baik et al. [21] also computed a cell size based on finite element modeling which agrees well with the experimental results.

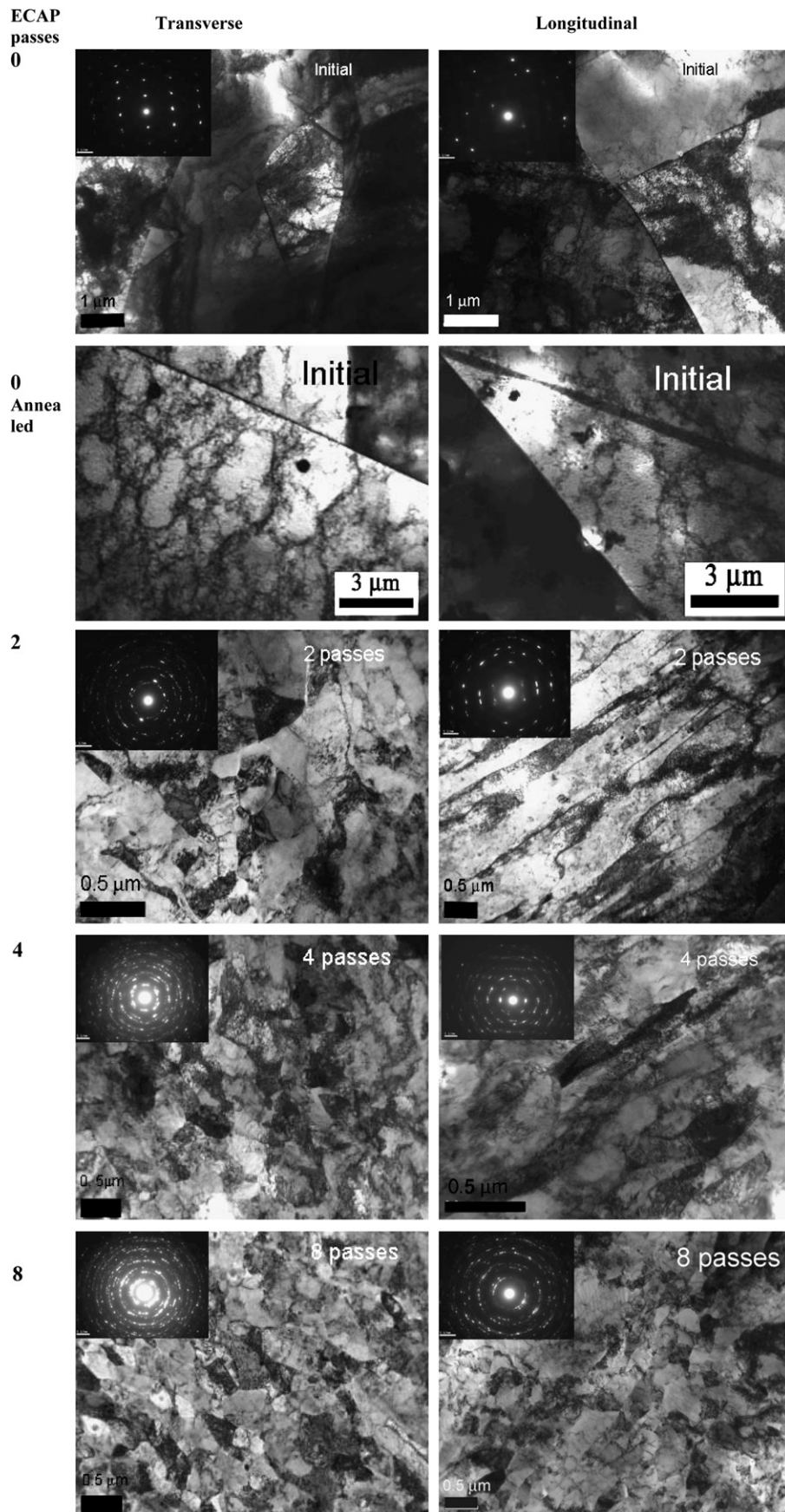


Fig. 6. TEM images of the ECAP Cu samples in longitudinal and transverse sections after 0, 0 (annealed), 2, 4 and 8 passes.

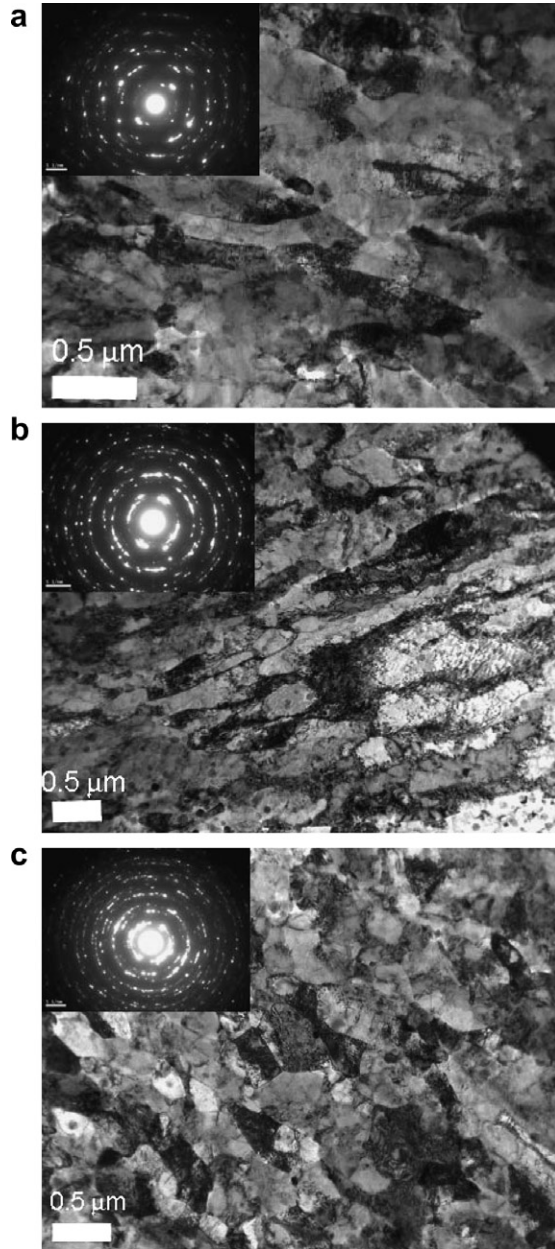


Fig. 7. Transverse images of ECAP Cu after 8 passes using three different routes: (a) Route A, (b) route C, and (c) route B_C.

We computed the approximate dislocation densities as a function of the number of ECAP passes. The results are presented in Fig. 10b and compared with X-ray measurements by Ungar and Zehetbauer [17] and Zehetbauer et al. [18,19]. Considering the uncertainty of TEM dislocation density measurements, the agreement can be considered very good.

The contribution of cell boundaries is not just to the dislocation density; as they become gradually sharper, they act as barriers to dislocation motion and gain a grain-boundary character. An alternative constitutive description is one in which the cell boundaries become gradually more impenetrable to dislocations. This can be represented by a Hall–Petch type expression:

$$\sigma_y = k_1 \alpha G b \rho_c^{1/2} + \frac{k_2}{d^x t^y}. \quad (4)$$

The first term represents the dislocation density evolution in the cell interiors and is identical to the first term in Eq. (3). The second term is a Hall–Petch type expression in which the cell size, d , has an exponent x . It is found (e.g. [37]) that $x = -1$ for cells. The expression t^y represents the contribution of the cell boundary thickness. As this thickness decreases, it becomes a more effective barrier. In the lower limit, $t \approx 0.5\text{--}1$ nm and the term k_2/t^y represents the Hall–Petch coefficient of d . The evolution of cell size thickness as a function of strain can be represented by:

$$t \text{ (nm)} = 1 + \left(\frac{k_3}{\gamma}\right)^2. \quad (5)$$

From the above equation, it can be seen that the cell wall thickness is infinity at small strains, and asymptotically approaches 1 nm at very high strains, which is a reasonable estimate. Using the above expression, Eq. (4) can be used to estimate the values of yield stress as a function of shear strain. The following values were used to compare predictions from Eq. (4) with experimental results:

$$\begin{aligned} k_1 &= 6.22 \\ k_2 &= 0.685 \text{ nm}^{1/2} \\ k_3 &= 0.0878 \times 10^{-9} \text{ MPa m}^{3/2} \\ \alpha &= 0.25 \\ G &= 42.1 \text{ GPa} \\ b &= 2.56 \times 10^{-10} \text{ m} \end{aligned}$$

A reasonably good agreement is found, indicating that cell boundaries do play a critical role in determining the yield strength of ultrafine-grained metals (see Fig. 11).

3.4. Comparison of ECAP with shear localization

The similarity between the microstructures produced by ECAP and the ones generated within adiabatic shear bands is striking, in spite of the significant differences in thermomechanical history. For comparison purposes, Fig. 12b shows the ultrafine grain sizes obtained in a hat-shaped specimen which constrained the plastic deformation in a narrow region with thickness of approximately 200 μm [38]. The shear strain imparted dynamically was approximately equal to 4. A grain size of 100–200 nm was produced. Fig. 12a shows the ECAP structure with equivalent shear strain (4 passes). The grain size is fairly similar, with a greater grain-boundary waviness observed after ECAP, shown by Mishra et al. [39]. This is indeed surprising, considering the major differences in strain rate (approximately 1 s⁻¹ for ECAP and 10⁴ s⁻¹ for the hat-shaped specimen) and thermal history (successive thermal spikes after each pass for ECAP and adiabatic heating to $T = 600$ K for the hat-shaped specimen).

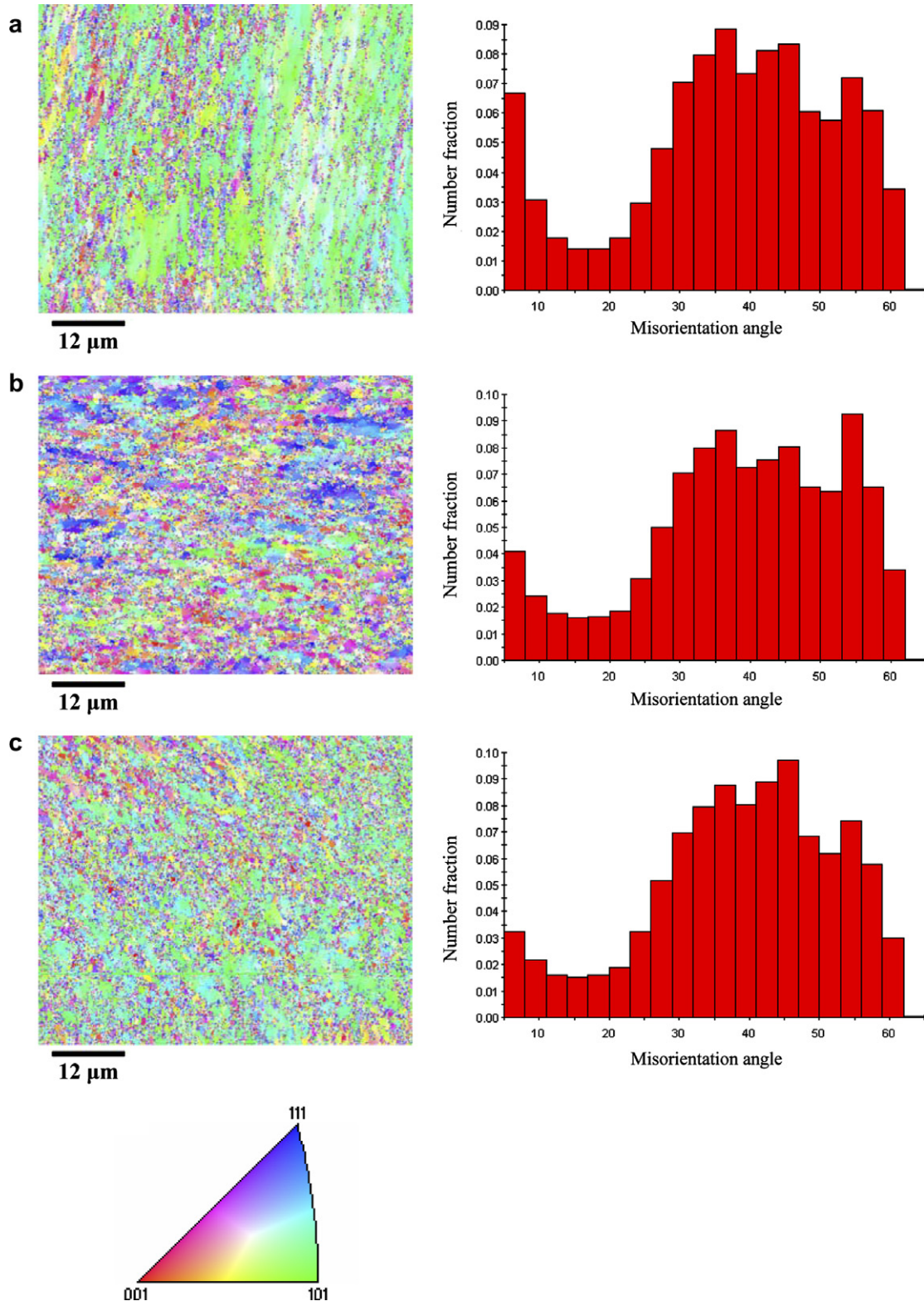


Fig. 8. EBSD pattern and misorientation angle distribution of ECAP Cu samples after 8 passes using three different routes; (a) route A, (b) route C, and (c) route B_C.

The similarity is made clear if one compares the Zener–Hollomon parameters, Z , for the two processes. This parameter incorporates both temperature, T , and strain rate, $\dot{\epsilon}$, into a unified expression which contains the activation energy for diffusion, Q [41]:

$$\ln Z = \ln \dot{\epsilon} + \frac{Q}{RT}. \quad (6)$$

For shear band formation, the strain rate is approximately equal to $10^4/\text{s}$. Using $Q = 72.5 \text{ kJ/mol}$ (the activation

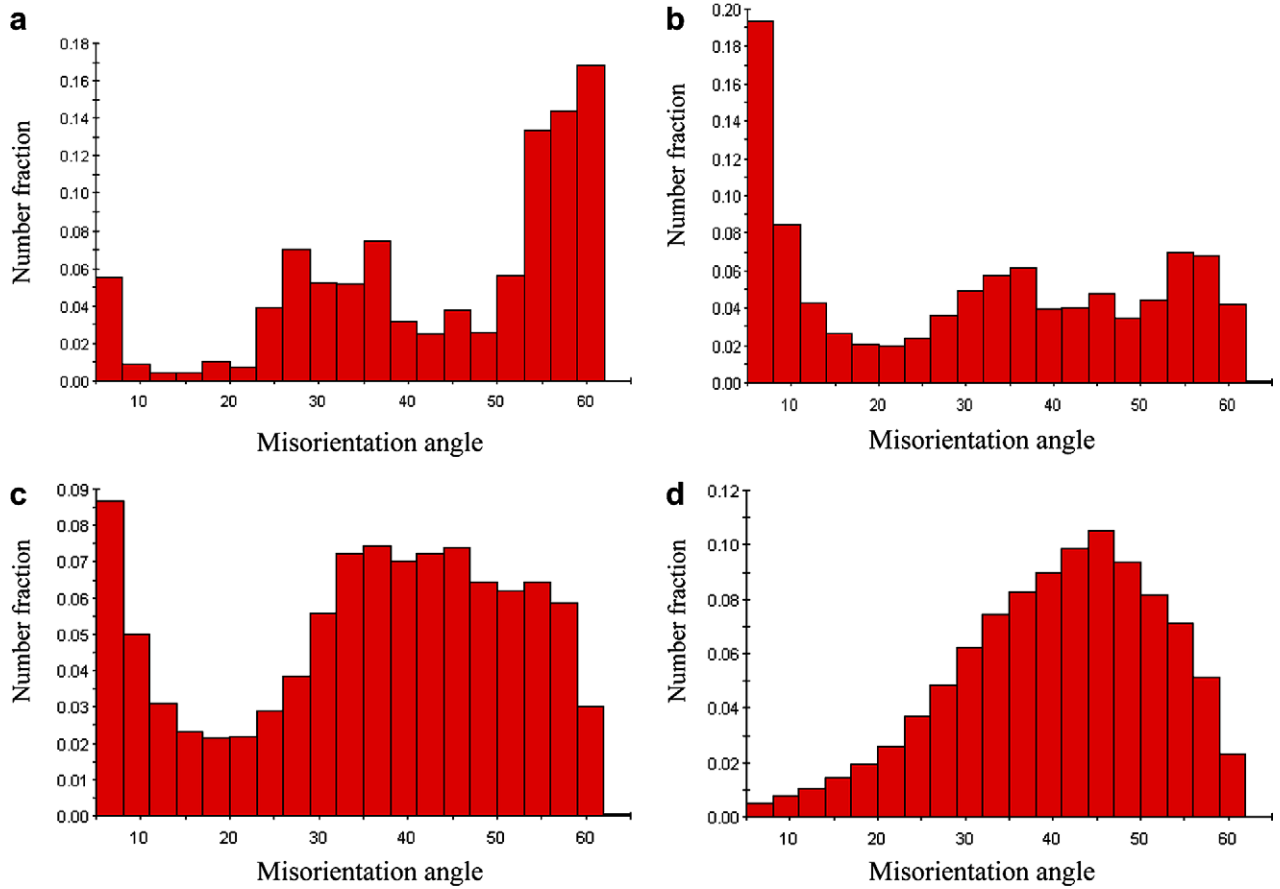


Fig. 9. Misorientation angle vs number fraction of grains for ECAP Cu samples with different number of ECAP passes (route B_C); (a) initial, (b) 2 passes, (c) 4 passes, and (d) 8 passes.

energy for grain-boundary diffusion in copper) and an estimated temperature $T = 500$ K, one obtains $\ln Z = 27$. For ECAP, the strain rate is approximately 1/s. The temperature rise is much more modest. We take, as a first approximation, $T = 350$ K (this is calculated in Section 3.5.1). Using the same activation energy, one obtains $\ln Z = 25$. Thus, the conditions in both adiabatic shear localization and ECAP favor some process of thermal recovery. The closeness of the values explains the similarity in microstructures.

3.5. Deformation-induced heating

The calculations were performed for the two deformation regimes; ECAP and dynamic deformation/adiabatic shear band. As shown in Section 3.4, these two deformation regimes have almost identical Zener–Hollomon parameters.

3.5.1. ECAP

The temperature rise during ECAP is an important factor in determining the deformation mechanism. As a first step, we calculated the temperature increase for our ECAP samples using the following equation:

$$\Delta T = \frac{\beta}{\rho C_v} \int_{\varepsilon_1}^{\varepsilon_2} \sigma d\varepsilon, \quad (7)$$

in which $\beta = 0.9$ (assuming 90% of work of deformation was converted to heat), ρ is the density of sample, and C_v is the specific heat capacity. The Voce equation was used for stress, leading to

$$\Delta T = \frac{\beta}{\rho C_v} \int_{\varepsilon_1}^{\varepsilon_2} \left[\sigma_s + (\sigma_0 - \sigma_s) \exp\left(-\frac{\varepsilon}{\varepsilon_0}\right) \right] d\varepsilon, \quad (8)$$

ΔT as a function of number of passes is plotted in Fig. 13a. From our calculation, ΔT saturates to 55 K after ~ 6 passes. It should be noted that the calculation above assumes adiabaticity of the thermal deformation process. This assumption is justified if the thermal diffusion length is much smaller than the dimensions of the system enclosure. Indeed, calculating thermal diffusion length using $x = \sqrt{\alpha t}$, where in our case $\alpha = 0.08$ cm²/s is the thermal diffusivity of steel, and t is the time of deformation (~ 0.1 s), we get $x = 0.09$ mm, which is much smaller than the cross-sectional dimension of the specimen (9 mm).

A two-dimensional steady-state conduction equation was applied to estimate the cooling time for the extruded sample:

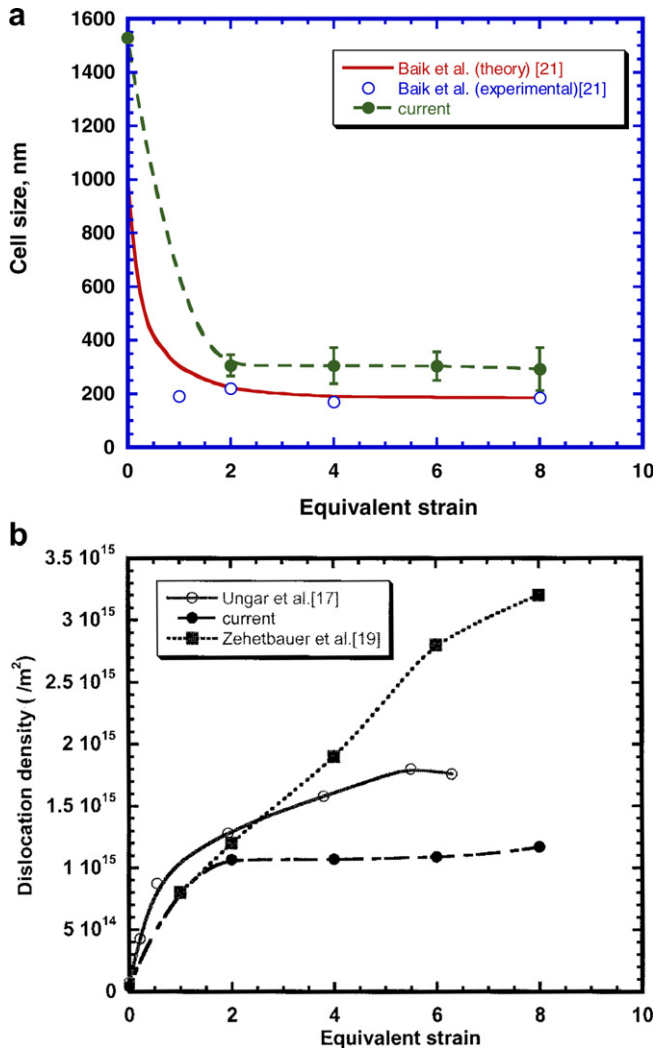


Fig. 10. (a) Prediction of cell size as a function of equivalent strain by Baik et al. [21] (measured and calculated) and current results; (b) prediction of dislocation density as function of equivalent strain by Ungar and Zehetbauer [17], Zehetbauer and Seumer [19] and current results.

$$\rho CV \frac{dT}{dt} = Sk\Delta T_{1-2}, \quad (9)$$

where ρ , C and V are the density, specific heat capacity and volume of the copper rod, S is the conduction shape factor for the case of a circular cylinder centered in a square solid of equal length, k is the thermal conductivity of steel in which the copper rod is embedded, and ΔT_{1-2} is the temperature difference between the copper rod and the steel die, the latter being at room temperature, 300 K.

For our case, $\rho = 8890 \text{ kg/m}^3$, $C = 380 \text{ J/kg K}$, $V = 3.98 \times 10^{-6} \text{ m}^3$, $S = 0.066$, $k = 35.17 \text{ W/m K}$, $T_2 = 300 \text{ K}$.

Using the above values, and integrating Eq. (9), we get:

$$T (\text{K}) = 300 + 55 \exp(-0.247t). \quad (10)$$

The plot of temperature vs. time using the above equation is shown in Fig. 13b. From the plot, it can be seen that in $\sim 5 \text{ s}$, the sample cools down to room temperature.

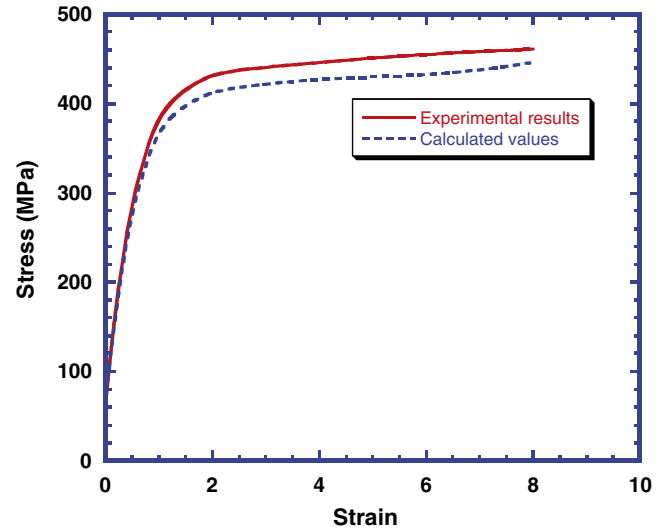


Fig. 11. Yield stress as a function of shear strain from experiments and calculated values using Eq. (4).

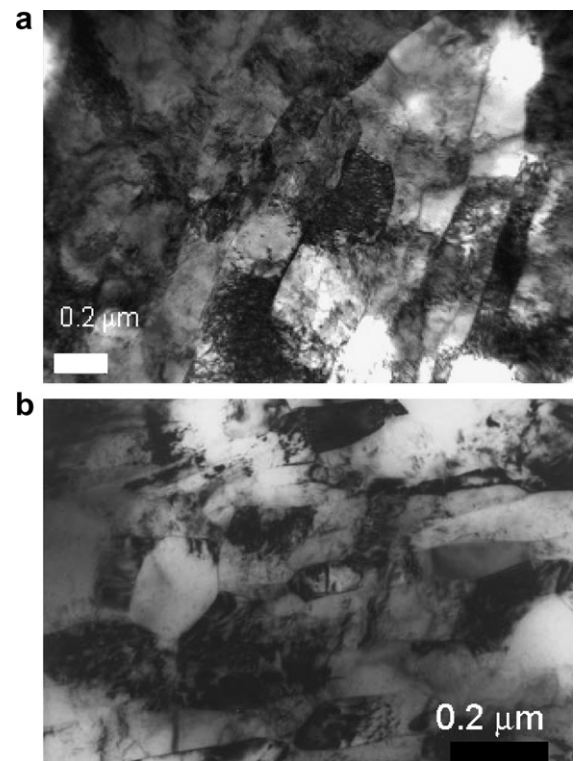


Fig. 12. TEM micrographs of Cu subjected to shear strain of 4; (a) ECAP: 4 passes ($\sim \dot{\gamma} \approx 1 \text{ s}^{-1}$); (b) hat-shaped specimen ($\dot{\gamma} \approx 10^4 \text{ s}^{-1}$).

3.6. Modeling of microstructural evolution

Fig. 14 shows a schematic describing, in a simplified way, the evolution of the microstructure leading to the ultrafine grain size. A similar sequence was also proposed by Xu et al. [24] and Mishra et al. [40] for ECAP and Andrade et al. [38] and Meyers et al. [53] for adiabatic shear bands. One starts with a random dislocation distribution

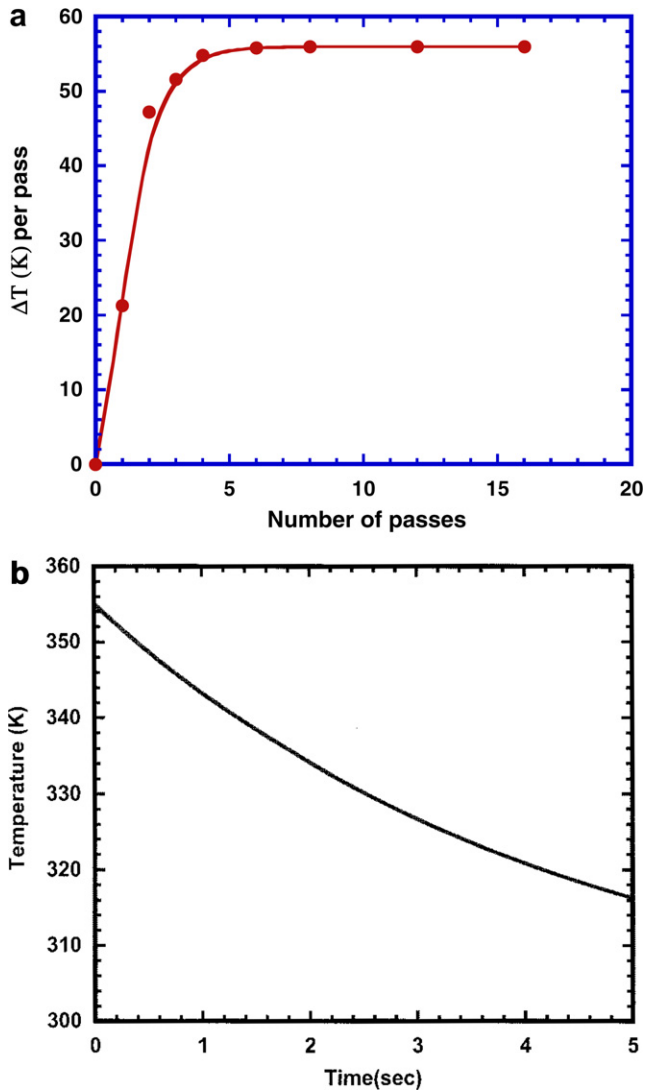


Fig. 13. (a) Temperature rise as a function of number of ECAP passes; (b) cooling rate of ECAP samples.

(Fig. 14a), which is not a low-energy configuration. This random distribution gives way to elongated cells, such as the ones shown in Fig. 5 (longitudinal section). The energetics of this process was analyzed by Meyers et al. [43,44], among others. This stage is shown in Fig. 14b. As the deformation continues and as the misorientation increases, these cells become elongated subgrains (Fig. 14c). These elongated structures are seen in many metals subjected to high strains, as reported by, e.g. Gil Sevillano et al. [45]. Hughes and Hansen [46] reported rotations of 30–45° at medium and large strains (cold rolling reductions from 70% to 90%). Hughes et al. [47] made detailed TEM observations on heavily deformed Ta and found evolution from configuration b to c in Fig. 14. Similar observations and analyses were made by Hansen, Kuhlmann-Wilsdorf and co-workers [48–51]. These elongated subgrains are, in their turn, plastically deformed, leading to further breakup (Fig. 14d). Eventually, the elon-

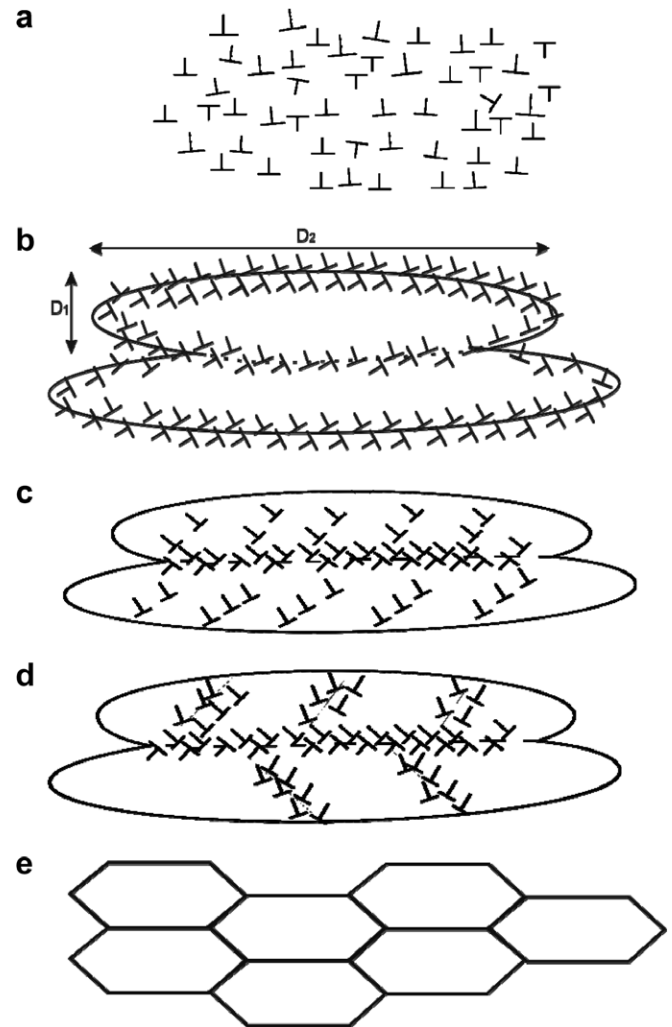


Fig. 14. Schematic illustration of microstructural evolution during severe plastic deformation. (a) Homogeneous distribution of dislocations; (b) elongated cell formation; (c) dislocations blocked by subgrain boundaries; (d) break up of elongated subgrains; and (e) reorientation of subgrain boundaries and formation of ultrafine grain size.

gated subgrains break up into approximately equiaxed micrograins (Fig. 14e). This sequence of events, which is well known for severe plastic deformation, has been given different names:

- Rotational dynamic recrystallization (e.g. Derby [52]), which needs concurrent plastic deformation, is well documented for geological materials. This was the interpretation given in adiabatic shear bands by Meyers et al. [42,53] for titanium, Andrade et al. [38] for copper and Nesterenko et al. [54] for tantalum.
- Formation of geometrically necessary boundaries [47–51,55,56].
- Continuous recrystallization [57,58].

Once this equiaxed ultrafine grain structure is achieved, it has to undergo additional plastic deformation under the imposed conditions. Although this area is still being inves-

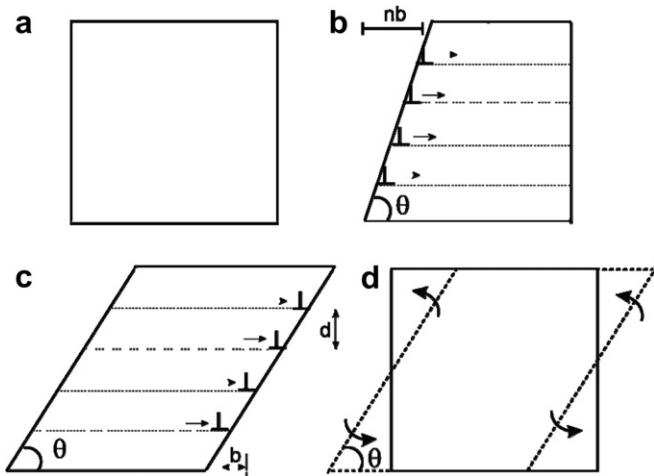


Fig. 15. Sequential plastic deformation and grain-boundary rotations yielding steady state ultra-fine equiaxed grains; (a) initial cubic grain configuration; (b) slip by dislocation emission from grain boundaries; (c) annihilation at opposite boundary; (d) deformed grain subjected to grain-boundary rotations leading to original grain configuration that will, in turn, be deformed by slip.

tigated, a possible mechanism is presented in Fig. 15. As the grain size is reduced to the 50–200 nm range, the deformation mechanisms operating at conventional grain sizes

have to be re-examined. The concept of grain-boundary sources and sinks in the deformation of nanocrystalline metals was identified in molecular dynamics simulations [59,60]. We assume that grain-boundaries act as primary sources of dislocations, as shown in Fig. 15b. There is an associated shear of the idealized cubic ultrafine grain, when the dislocations move across the grains and are annihilated in the opposite boundary (Fig. 15c). The cube is transformed into a parallelepiped. In order for the equiaxed morphology to be retained, it is necessary for the grain boundaries to rotate back to their initial configuration. It will be demonstrated below that this process can occur during plastic deformation, as is shown schematically in Fig. 15d. This rotation of the grain boundaries, coupled with shear on a new slip plane, ensures the retention of a steady-state equiaxed structure (Fig. 15a).

The rotation of grain boundaries is a diffusion-controlled process that would not be possible for conventional grain sizes. Two calculations are given below which show that these movements can indeed take place during or immediately after deformation. The first of these calculations was developed earlier to explain the ultrafine equiaxed structures inside adiabatic shear bands. The second grain-boundary mobility calculation is based on grain-boundary curvature.

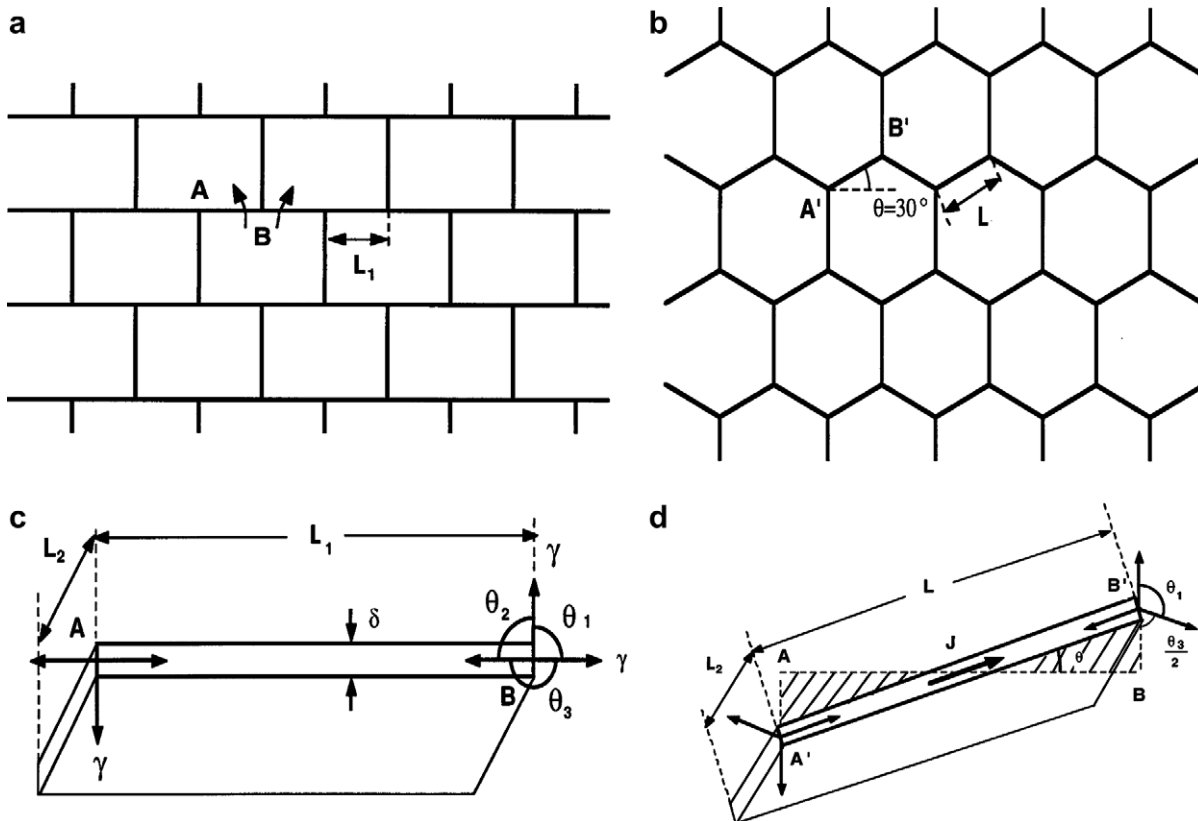


Fig. 16. Rotation of grain boundaries leading to equiaxed configuration (a) a grain boundary AB under effect of interfacial energies; (a) initial configuration after breakup of elongated subgrains; (b) configuration after rotation of boundary segments; (c) material flux through grain boundary diffusion and rotation of AB to A'B'; and (d) predicted rotation as a function of time for $L = 200$ nm and three temperatures.

3.6.1. Grain-boundary rotation analysis

The process of grain-boundary rotation during deformation was analyzed by Meyers et al. [43]. It is reproduced here briefly. In order for this mechanism to be viable, it has to be shown that grain-boundary rotation can be accomplished within the time/temperature window created by plastic deformation. The relaxation of the rotated grains into a more equiaxed microcrystalline structure can occur by minor rotations of the grain boundaries. Fig. 16a and b shows that a rotation of 30° of the boundaries transforms elongated/segmented subgrains into an equiaxed structure. If each longitudinal grain boundary segment AB rotates to A'B' by an angle θ , the original equiaxed structure will be created. This is illustrated in Fig. 16c and d. Such a rotation can be accomplished by the flux of atoms along the grain boundary, which can occur at rates that are orders of magnitude higher than in the bulk. The activation energy for grain boundary diffusion is approximately one-half of that for lattice diffusion [61,62]. A general form of Fick's law expressed in terms of a potential energy gradient has to be used [62]. This is a critical element of the model: a mechanical stress induces diffusion. We start with force \vec{F} , acting on a particle:

$$\vec{F} = \nabla V, \tag{11}$$

where ∇V is the gradient of the potential energy field. The mean diffusion velocity \vec{v} is the product of the mobility M by this force: $\vec{v} = M\vec{F}$. The flux along a grain boundary with thickness δ and depth L_2 (cross-sectional area $L_2\delta$) is:

$$J = L_2\delta CMF = \left(\frac{L_2\delta DC}{kT}\right)F, \tag{12}$$

where D is the diffusion coefficient and C is the concentration of the mobile species (expressed in terms of mass per unit volume).

The rotation of the boundaries is driven by the minimization of the interfacial energy (e.g. Murr [62]). The force exerted by the grain boundaries is represented in Fig. 16c and is equal to:

$$F = \gamma \left(1 - 2 \cos \frac{\theta_3}{2}\right) L_2. \tag{13}$$

The relationship between the grain boundary rotation and the volume flow, dV , required through the mid-point of the grain boundary AB is (computed per thickness, L_2):

$$\frac{L^2 d\theta}{4L_2} = dV, \tag{14}$$

where dV is the volume transferred and L is the instantaneous length of the segment A'B' (Fig. 16b). But:

$$L = \frac{L_1}{\cos \theta}, \tag{15}$$

where L_1 is the initial length, or AB. Thus

$$\frac{d\theta}{dt} = \frac{4 \cos^2 \theta}{L_2 L_1^2} \frac{dV}{dt} = \frac{4 \cos^2 \theta}{L_2 L_1^2 \rho} \frac{dm}{dt}, \tag{16}$$

where dm/dt is the mass change, which is the rate of volume change multiplied by ρ , the density.

The rate of mass change is the flux, and we have, substituting Eq. (12):

$$\frac{d\theta}{dt} = \frac{4 \cos^2 \theta}{L_2 L_1^2 \rho} J = \frac{4 \cos^2 \theta}{L_2 L_1^2 \rho} \left(\frac{L_2 \delta DC}{kT}\right) F \tag{17}$$

$$\frac{d\theta}{dt} = \frac{4 \cos^2 \theta}{L_1^2 \rho} \frac{\delta DC}{kT} \gamma (1 - 2 \sin \theta) L_2. \tag{18}$$

We consider equiaxed grains and $L_2 \approx L_1$.

$$\frac{4\delta D\gamma}{L_1 kT} t = \int_0^\theta \frac{d\theta}{\cos^2 \theta (1 - 2 \sin \theta)}. \tag{19}$$

Integrating, we arrive at

$$\frac{\tan \theta - \frac{2}{3} \cos \theta}{(1 - 2 \sin \theta)} + \frac{4}{3\sqrt{3}} \ln \frac{\tan \frac{\theta}{2} - 2 - \sqrt{3}}{\tan \frac{\theta}{2} - 2 + \sqrt{3}} + \frac{2}{3} - \frac{4}{3\sqrt{3}} \ln \frac{2 + \sqrt{3}}{2 - \sqrt{3}} = \frac{4\delta D\gamma}{L_1 kT} t. \tag{20}$$

A step-by-step derivation is provided by Meyers et al. [63]. The most important parameter in Eq. (20) is the

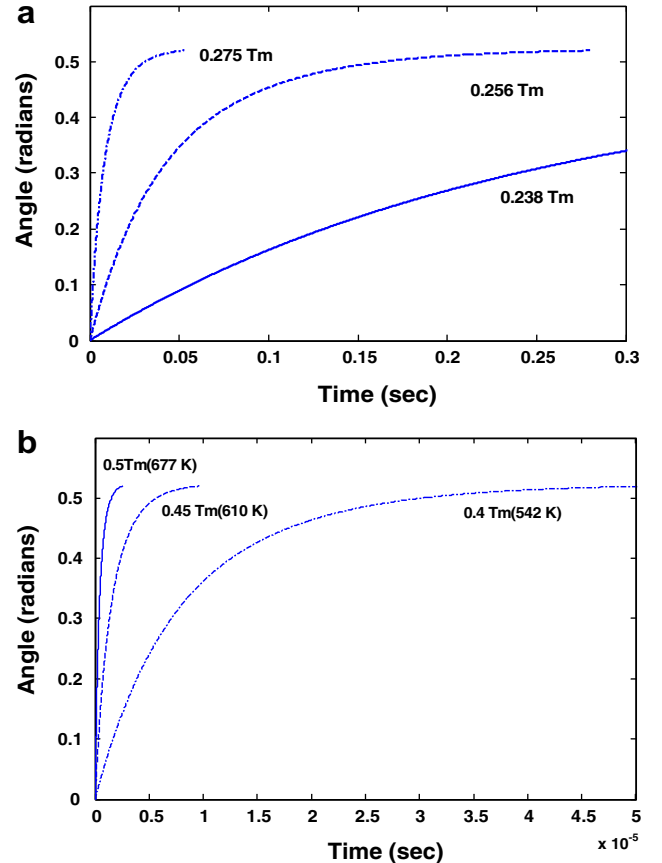


Fig. 17. Predicted angle of rotation for copper versus time for copper in (a) ECAP, (b) shear band formation.

grain-boundary diffusion coefficient. These values were obtained experimentally by Surholt and Herzig [64]:

$$\delta D_{GB} = 3.9 \times 10^{-16} \exp \left[\frac{-72.5 \text{ kJ/mol}}{RT} \right] (\text{m}^3/\text{s}). \quad (21)$$

3.6.1.1. ECAP. For grain rotation calculation, the grain size diameter for ECAP is taken as $0.2 \mu\text{m}$. For $T/T_m = 0.238, 0.256, 0.275$, the plots are given in Fig. 17a. For $0.275T_m$, rotation of grains by 30° takes place in ~ 50 ms. At $0.238T_m$ there is a significant drop in the rotation angle (17°) over an estimated time of ~ 300 ms. Using values of grain boundary diffusion coefficient and activation energy from Gust et al. [65], we obtain higher values for rotation time for both shear band and ECAP processes. For example, with these modified values we get a rotation time of $\sim 20 \mu\text{s}$ for 30° rotation in shear band formation while it now takes 30 s for 30° rotation in ECAP at $0.275T_m$. The grain-boundary width, variously taken as $0.5\text{--}1$ nm, is not needed, since it is embedded into Eq. (21). The interfacial energy was obtained from Murr [62], and is taken as 0.725 mJ/m^2 . The rate of rotation decreases with increasing θ and asymptotically approaches 30° as $t \rightarrow \infty$.

3.6.1.2. Dynamic deformation/adiabatic shear band formation. As in the case of ECAP, a grain size diameter of $0.2 \mu\text{m}$ was used with three different values of temperature ($0.4, 0.45$ and $0.5T_m$). Fig. 17b shows that for $0.5T_m$, grain rotation of 30° takes place in less than 1 ms, while with decreasing temperature, this rotation takes progressively longer. For example, for a rotation of 30° , it takes $\sim 5 \mu\text{s}$ at $0.4T_m$ as compared to $<1 \mu\text{s}$ at $0.5T_m$. The calculations predict significant rotations of the boundary within the deformation time ($\sim 50\text{--}100 \mu\text{s}$) at temperatures between 0.45 and $0.5T_m$, for micrograin sizes of $0.1\text{--}0.3 \mu\text{m}$. Thus, the reorientation of grain boundaries can take place during plastic deformation. This does not exclude the possibility of reorientation/accommodation of the grain boundaries during cooling. As discussed earlier, for ECAP where the process is much slower and the temperature rise is significantly lower, it takes much longer for grain rotation to proceed to the same extent.

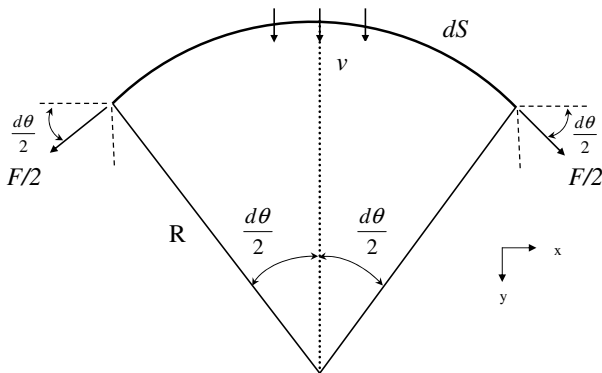


Fig. 18. Schematic showing force acting on the grain boundary with radius of curvature R .

3.6.2. Grain boundary mobility

A second, simpler approach to the grain-boundary rotations required to maintain an equiaxed structure is given below. It was inspired by a lecture given by Li [67] and by experiments by Rath and Hu [68]. The driving force on a grain-boundary can be simply estimated by equating the force acting on a curved segment of dS due to the grain-boundary energy, γ . The total force acting on the grain boundary in the y -direction (Fig. 18) is:

$$F = 2\gamma \sin \frac{d\theta}{2} \approx \gamma d\theta \quad (\text{since } \theta \text{ is considered small}). \quad (22)$$

Therefore,

$$\text{force/area} = \frac{\gamma d\theta}{Rd\theta} = \frac{\gamma}{R}. \quad (23)$$

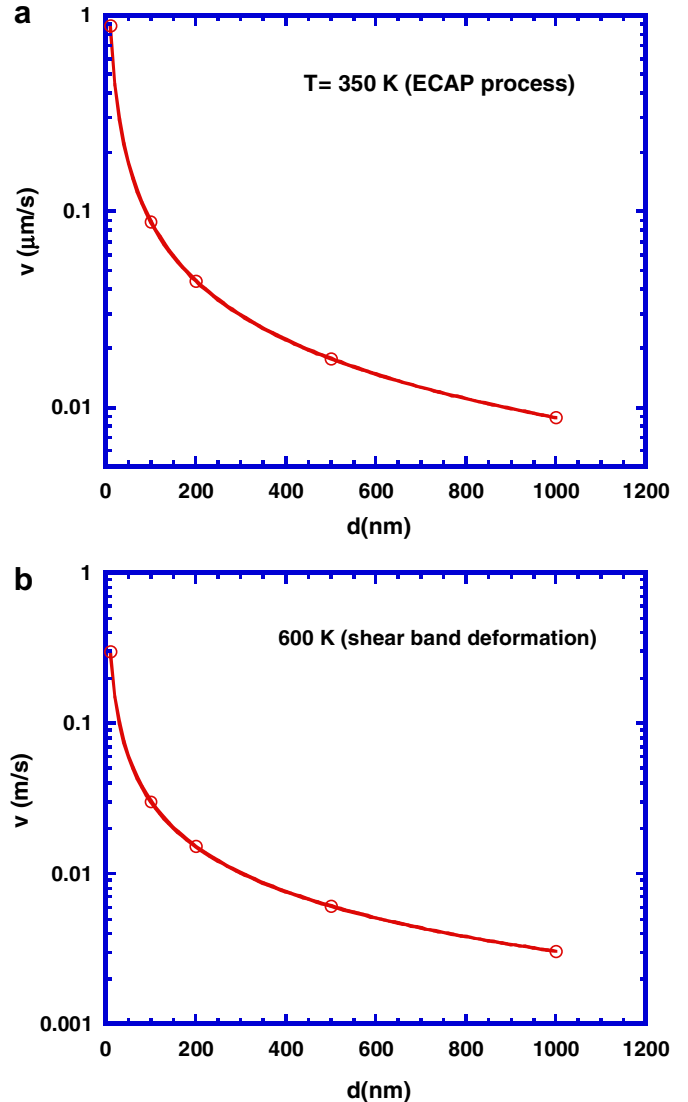


Fig. 19. Grain boundary velocity as a function of grain size for two different temperatures: (a) 350 K, typical of ECAP process; (b) 600 K, typical of shear band deformation process.

The velocity of the grain boundary is proportional to the force acting on the segment dS :

$$v \propto \frac{\gamma}{R} = M \frac{\gamma}{R}, \quad (24)$$

where M , grain boundary mobility, is the proportionality constant. The mobility has an Arrhenius-type temperature dependence [57].

$$M = M_0 \exp\left(\frac{-Q}{RT}\right). \quad (25)$$

For copper [66]: $M_0 = 7.5 \times 10^6$ m/s and $Q = 121$ kJ/mol.

Assuming $d/2 = R$, where d is the grain size, grain boundary velocity is plotted against grain size in Fig. 19a and b for two different temperatures, 350 and 600 K. For $d = 200$ nm (the limit of grain size achieved in ECAP), $v = 40$ nm/s. A similar plot at 600 K, typical of shear band deformation process, indicates velocity to be higher by a factor of 6. From Fig. 13b, it can be seen that the cooling to 345 K occurs inside the ECAP die in a time of the order of 1 s. Thus, a grain boundary movement of 40 nm can be expected in this time. This could be sufficient to reorganize the deformation grain configuration.

In contrast, for a shear band the cooling takes place in timescales of fractions of a millisecond. For 0.1 ms and a grain size of 200 nm ($v = 0.01$ m/s), a displacement of 10 nm is obtained. Again, this is a reasonable value for the rotation of the deformed grain boundaries.

Thus, this simple mobility calculation confirms the more elaborate analysis of Section 3.6.1. Rath and Hu [68] use a similar expression except for the exponent, m in their expression, which depends on the grain boundary misorientation and grain boundary purity:

$$v = M \cdot \Delta F^m = M \left(\frac{\gamma}{R}\right)^m. \quad (26)$$

In their experiments, m varies from 1 to 4. This can be attributed to grain boundary solutes and misorientation.

3.6.3. Additional considerations

There is a dearth of information on grain-boundary mobility in nanocrystalline and ultrafine-grained metals. Nevertheless, recent experiments seem to indicate that it is much higher than for conventional grain sizes. It should be mentioned that Li [69] has recently proposed an alternative mechanism through which boundaries, comprised of dislocation arrays, migrate through the glide of dislocations. This analysis by Li is based on observations by Zhang et al. [70,71] of grain growth in nanocrystalline copper under high stresses at 83 K. In a recent publication, Liao et al. [73] reported that above a critical stress value, deformation-induced grain growth can take place in electrodeposited nanocrystalline Ni during high-pressure torsion. Interestingly, the grain sizes of conventional specimens are reduced to the ~ 200 nm range by high-pressure torsion, while the grain sizes of nanocrystalline Ni is increased to ~ 200 nm by the same deformation process.

4. Conclusions

The thrust of the work reported herein was to explain the mechanism of deformation during severe plastic deformation. In order to accomplish this, ECAP were carried out on copper in three modes: A, C and B_C. The B_C sequence led to the most equiaxed ultrafine grain structure with size in the 0.2–0.5 μm range. The mechanical response of ECAP samples is shown to be captured well by the Voce equation which predicts saturation in yield strength of approximately 450 MPa, consistent with results in the literature. It was shown through EBSD that significant grain rotation can take place during the process of deformation in ECAP. For the first passes, a significant fraction of boundaries is low angle. As the number of passes increases, the fraction of large-angle boundaries increases. For eight passes, the grain-boundary misorientation distribution is similar to the starting material.

ECAP is compared with adiabatic shear band formation during high-strain rate deformation, and it is shown that the two processes have significantly different strain rates and temperatures but similar Zener–Hollomon parameters that lead to similar ultrafine grain structures. Calculations predict a temperature rise of ~ 55 K in the ECAP process, after two passes and cooling of these samples to room temperature in times on the order of 1 s, which is sufficient for grain segments of 0.5 μm to rotate by a grain-boundary diffusion mechanism. This mechanism was originally proposed for high-strain, high-strain rate deformation and was found to be applicable to ECAP.

It is proposed that the retention of a steady-state grain size (~ 200 nm) and equiaxed grain configuration is ensured by successive deformation and grain boundary reorientation. The plastic deformation elevates the temperature sufficiently (to ~ 350 K) in ECAP to enhance grain-boundary mobility to the extent that the grain boundaries can reorient themselves after plastic deformation and the material can subsequently retain its equiaxed structure. The grain-boundary reorientation as a function of time is calculated for different grain sizes and it is shown that, for $d \approx 200$ nm, this reorientation, corresponding to a rotation of $\sim 30^\circ$, can occur within the timescale of post-deformation cooling. A simpler mobility calculation was also performed which confirms the more elaborate grain-boundary rotation calculation.

In conclusion, although the exact mechanisms of grain refinement are not completely understood, it is becoming obvious that grain-boundary mobility, including rotation, plays an important role during plastic deformation of ultra-fine grained metals.

Acknowledgements

This work was supported by the National Science Foundation under Grant CMS-0210173 (NIRT). We thank Professors R.J. Asaro and T. Langdon for helping us with the ECAP unit and Professor M.E. Kassner for fruitful

discussions. Mr. F. Grignon was instrumental in the development of the ECAP procedure. Discussions with Professor J.C.M. Li led to the boundary mobility calculations presented herein.

References

- [1] NanoSPD1, Moscow; 1999.
- [2] Zehetbauer Michael, Valiev Ruslan Z, editors. Nanomaterials by severe plastic deformation. Proceedings of NanoSPD2, Vienna; 2002.
- [3] Horita Z, editor. Nanomaterials by severe plastic deformation. Proceedings of NanoSPD3, Fukuoka; 2005.
- [4] Furukawa M, Horita Z, Nemoto M, Langdon TG. *J Mater Sci* 2001;36:2835.
- [5] Valiev RZ, Krasilnikov NA, Tsenev NK. *Mater Sci Eng A* 1991;137:35.
- [6] Valiev RZ, Kozlov EV, Ivanov YUF, Lian J, Nazarov AA, Budalet B. *Acta Metall Mater* 1994;42:2467.
- [7] Wang J, Furukawa M, Horita Z, Nemoto M, Valiev RZ, Langdon TG. *Mater Sci Eng A* 1996;216:41.
- [8] Wang J, Iwahashi Y, Horita Z, Furukawa M, Nemoto M, Valiev RZ, et al. *Acta Mater* 1996;44:2973.
- [9] Furukawa M, Ma Y, Horita Z, Nemoto M, Valiev RZ, Langdon TG. *Mater Sci Eng A* 1998;241:122.
- [10] Iwahashi Y, Horita Z, Nemoto M, Langdon TG. *Acta Mater* 1997;45:4733.
- [11] Ferrasse S, Segal VM, Hartwig KT, Goforth RE. *Metall Mater Trans A* 1997;28:1047.
- [12] Iwahashi Y, Horita Z, Nemoto M, Langdon TG. *Acta Mater* 1998;46:3317.
- [13] Furukawa M, Iwahashi Y, Horita Z, Nemoto M, Langdon TG. *Mater Sci Eng A* 1998;257:328.
- [14] Langdon TG, Furukawa M, Nemoto M, Horita Z. *JOM* 2000;52:30.
- [15] Oh-Ishi K, Horita Z, Furukawa M, Nemoto M, Langdon TG. *Metall Mater Trans A* 1998;29:2011.
- [16] Pragnell PB, Gholinia A, Markushev VM. In: Lowe TC, Valiev RZ, editors. Investigations and applications of severe plastic deformation. Dordrecht: Springer; 2000. p. 65.
- [17] Ungar T, Zehetbauer M. *Scripta Mater* 1996;35:1467.
- [18] Zehetbauer M, Ungar T, Kral R, Borbely A, Schafner E, Ortner B, et al. *Acta Mater* 1999;47:1053.
- [19] Zehetbauer M, Seumer V. *Acta Mater* 1993;41:577.
- [20] Goerdeler M, Gottstein G. *Mater Sci Eng A* 2001;309:377.
- [21] Baik SC, Hellmig RJ, Estrin Y, Kim HS. *Z Metallkd* 2003;94:754.
- [22] Baik SC, Estrin Y, Hellmig RJ, Jeong HT, Brokmeier HG, Kim HS. *Z Metallkd* 2003;94:1189.
- [23] Toth LS, Molinari A, Estrin Y. *J Eng Mater Technol* 2002;124:71.
- [24] Xu C, Furukawa M, Horita Z, Langdon TG. In: Horita Z, editor. Nanomaterials by severe plastic deformation, Fukuoka, Japan; 2005. p. 19.
- [25] Krishnaiah A, Chakkingal U, Venugopal P. In: Horita Z, editor. Nanomaterials by severe plastic deformation. Proceedings of NanoSPD3, Fukuoka, Japan; 2005. p. 733.
- [26] Kadri SJ, Hartwig KT. In: Horita Z, editor. Nanomaterials by severe plastic deformation. Proceedings of NanoSPD3, Fukuoka, Japan; 2005. p. 349.
- [27] Wang JT, Du ZZ, Kang F, Chen G. In: Horita Z, editor. Nanomaterials by severe plastic deformation. Proceedings of NanoSPD3, Fukuoka, Japan; 2005. p. 663.
- [28] Vinogradov A, Suzuki T, Hashimoto S, Kitagawa K, Kuznetsov A, Dobatkin S. In: Horita Z, editor. Nanomaterials by severe plastic deformation. Proceedings of NanoSPD3, Fukuoka, Japan; 2005. p. 971.
- [29] Molodova X, Bhaumik S, Winning M, Gottstein G. In: Horita Z, editor. Nanomaterials by severe plastic deformation. Proceedings of NanoSPD3, Fukuoka, Japan; 2005. p. 469.
- [30] Chinh NQ, Horváth G, Horita Z, Langdon TG. *Acta Mater* 2004;52:3555.
- [31] Feltham P, Meakin JD. *Philos Mag* 1957;2:105.
- [32] Gourdin WH, Lassila DH. *Acta Metall Mater* 1991;39:2337.
- [33] Wang S, Murr LE. *Metall* 1980;13:203.
- [34] Meyers MA, Andrade U, Chokshi AH. *Metall Mater Trans A* 1995;26:2881.
- [35] Armstrong RW. In: Bunshah RF, editor. Advances in materials research. New York: Interscience; 1971. p. 101.
- [36] Voce E. *Metallurgia* 1955;51:219.
- [37] Rack HJ, Cohen M. *Front Mater Sci* 1976:365.
- [38] Andrade UR, Meyers MA, Vecchio KS, Chokshi AH. *Acta Metall Mater* 1994;42:3183.
- [39] Mishra A, Richard V, Gregori F, Asaro RJ, Meyers MA. *Mater Sci Eng A* 2005;410:290.
- [40] Mishra A, Richard V, Gregori F, Kad B, Asaro RJ, Meyers MA. In: Horita Z, editor. Nanomaterials by severe plastic deformation. Trans Tech Switzerland; 2006. p. 19.
- [41] Zener C, Hollomon JH. *J Appl Phys* 1944;15:22.
- [42] Meyers MA, Pak HR. *Acta Metall* 1986;34:2493.
- [43] Meyers MA, LaSalvia JC, Nesterenko VF, Chen YJ, Kad BK. In: McNelley TR, editor. Recrystallization and related phenomena. Monterey: MIA; 1997. p. 27.
- [44] Meyers MA, Nesterenko VF, LaSalvia JC, Xue Q. *Mater Sci Eng A* 2001;317:204.
- [45] Sevillano JG, van Houtte P, Aernoudt E. *Prog Mater Sci* 1981;25:69.
- [46] Hughes DA, Hansen N. *Acta Mater* 1997;45:3871.
- [47] Hughes DA, Lebensohn RA, Wenk HR, Kumar A. *Proc Roy Soc Lon A* 2000;456:921.
- [48] Kuhlmann-Wilsdorf D, Hansen N. *Scripta Metall Mater* 1991;25:1557.
- [49] Bay B, Hansen N, Hughes DA, Kuhlmann-Wilsdorf D. *Acta Metall Mater* 1992;40:205.
- [50] Liu Q, Hansen N. *Scripta Metall Mater* 1995;32:1289.
- [51] Hughes DA, Chrzan DC, Liu Q, Hansen N. *Phys Rev Lett* 1998;81:4664.
- [52] Derby B. *Acta Metall* 1991;39:955.
- [53] Meyers MA, Subhash G, Kad BK, Prasad L. *Mech Mater* 1994;17:175.
- [54] Nesterenko VF, Meyers MA, LaSalvia JC, Bondar MP, Chen Y-J, Lukyanov YL. *Mater Sci Eng A* 1997;229:23.
- [55] Pe'rez-Prado MT, Gonzalez-Doncel G, Ruano OA, McNelley TR. *Acta Mater* 2001;49:2259.
- [56] Kim HS, Joo D-H, Kim M-H, Hwang S-K, Kwun S-I, Chae S-W. *Mater Sci Technol* 2003;19:403.
- [57] Humphreys FJ, Hatherly M. *Recrystallization and related annealing phenomena*. Oxford: Pergamon Press; 1995.
- [58] Pragnell PB, Hayes JS, Bowen JR, Apps PJ, Bate PS. *Acta Mater* 2004;52:3193.
- [59] Yamakov D, Wolf D, Phillpot SR, Mukherjee AK, Gleiter H. *Nat Mater* 2002;1:1.
- [60] Froese AG, Derlet H, Van Swygenhoven H. *Acta Mater* 2004;52:4025.
- [61] Shewmon PG. *Diffusion in solids*. 2nd ed. Warrendale (PA): TMS-AIME; 1989. p. 3.
- [62] Murr LE. *Interfacial phenomena in metals and alloys*. Reading (MA): Addison-Wesley; 1975.
- [63] Meyers MA, Voehringer O, Lubarda V. *Acta Mater* 2003;51:1307.
- [64] Surholt T, Herzig C. *Acta Mater* 1997;45:3817.
- [65] Gust W, Mayer S, Bögel A, Predel B. *J Phys C* 1985;46:537.
- [66] Haessner F, Hofmann S. In: Haessner F, Riederer Verlag DR, editors. Recrystallization of metallic materials, Stuttgart; 1978. p. 63.
- [67] Li JCM. TMS annual meeting; 2005, unpublished results.
- [68] Rath BB, Hu H. In: Hu H, editor. Nature and behaviour of grain boundaries. TMS Publication; 1972. p. 405.
- [69] Li JCM. *Phys Rev Lett* 2006;96:215506.
- [70] Zhang K, Weertman JR, Eastman JA. *Appl Phys Lett* 2004;85:5197.
- [71] Zhang K, Weertman JR, Eastman JA. *Appl Phys Lett* 2005;87.
- [72] Dalla Torre FH, Pereloma EV, Davies CHJ. *Acta Mater* 2006;54:1135.
- [73] Liao XZ, Kilmametov AR, Valiev RZ, Gao H, Li X, Mukherjee AK, et al. *Appl Phys Lett* 2006;88:021909.